

Physical aspects of magnetized Jeffrey nanomaterial flow with irreversibility analysis

Fazal Haqk, Muhammad Ijaz Khan, Sami Ullah Khan, Khadijah M Abualnaja, and M A El-Shorbagy

Citation: Chin. Phys. B, 2022, 31 (**8**): 084703. DOI: 10.1088/1674-1056/ac4236
Journal homepage: http://cpb.iphy.ac.cn; http://iopscience.iop.org/cpb

What follows is a list of articles you may be interested in

Three-dimensional MHD flow over a shrinking sheet: Analytical solution and stability analysis

Sumaira Afzal, Saleem Asghar, Adeel Ahmad
Chin. Phys. B, 2017, 26 (**1**): 014704. DOI: 10.1088/1674-1056/26/1/014704

Bifurcation phenomena and control for magnetohydrodynamic flows in a smooth expanded channel

G. C. Layek, Mani Shankar Mandal, H. A. Khalaf
Chin. Phys. B, 2014, 23 (**11**): 114701. DOI: 10.1088/1674-1056/23/11/114701

MHD boundary layer flow of Casson fluid passing through an exponentially stretching permeable surface with thermal radiation

Swati Mukhopadhyay, Iswar Ch, ra Moindal, Tasawar Hayat
Chin. Phys. B, 2014, 23 (**10**): 104701. DOI: 10.1088/1674-1056/23/10/104701

Existence of a Hartmann layer in the peristalsis of Sisko fluid

Saleem Asghar, Tayyaba Minhas, Aamir Ali
Chin. Phys. B, 2014, 23 (**5**): 054702. DOI: 10.1088/1674-1056/23/5/054702

MHD flow of nanofluids over an exponentially stretching sheet in a porous medium with convective boundary conditions

T. Hayat, M. Imtiaz, A. Alsaedi, R. Mansoor
Chin. Phys. B, 2014, 23 (**5**): 054701. DOI: 10.1088/1674-1056/23/5/054701

Physical aspects of magnetized Jeffrey nanomaterial flow with irreversibility analysis

Fazal Haq[1,†], Muhammad Ijaz Khan[2,3], Sami Ullah Khan[4], Khadijah M Abualnaja[5], and M A El-Shorbagy[6,7]

[1] *Department of Mathematics, Karakoram International University Main Campus, Gilgit* 15100, *Pakistan*
[2] *Department of Mathematics and Statistics, Riphah International University I*-14, *Islamabad* 44000, *Pakistan*
[3] *Department of Mechanics and Engineering Science, Peking University, Beijing* 100871, *China*
[4] *Department of Mathematics, COMSATS University Islamabad, Sahiwal* 57000, *Pakistan*
[5] *Department of Mathematics and Statistics, College of Science, Taif University, P. O. Box* 11099, *Taif* 21944, *Saudi Arabia*
[6] *Department of Mathematics, College of Science and Humanities in Al-Kharj, Prince Sattam bin Abdulaziz University, Al-Kharj* 11942, *Saudi Arabia*
[7] *Department of Basic Engineering Science, Faculty of Engineering, Menoufia University, Shebin El-Kom* 32511, *Egypt*

(Received 11 October 2021; revised manuscript received 5 December 2021; accepted manuscript online 11 December 2021)

This research presents the applications of entropy generation phenomenon in incompressible flow of Jeffrey nanofluid in the presence of distinct thermal features. The novel aspects of various features, such as Joule heating, porous medium, dissipation features, and radiative mechanism are addressed. In order to improve thermal transportation systems based on nanomaterials, convective boundary conditions are introduced. The thermal viscoelastic nanofluid model is expressed in terms of differential equations. The problem is presented via nonlinear differential equations for which analytical expressions are obtained by using the homotopy analysis method (HAM). The accuracy of solution is ensured. The effective outcomes of all physical parameters associated with the flow model are carefully examined and underlined through various curves. The observations summarized from current analysis reveal that the presence of a permeability parameter offers resistance to the flow. A monotonic decrement in local Nusselt number is noted with Hartmann number and Prandtl number. Moreover, entropy generation and Bejan number increases with radiation parameter and fluid parameter.

Keywords: Jeffrey nonmaterial, entropy generation, magnetohydrodynamics (MHD), Bejan number, porous medium, Brownian motion

PACS: 47.65.–d, 47.65.Gx, 96.12.St, 91.35.Dc **DOI:** 10.1088/1674-1056/ac4236

1. Introduction

Rheological behavior of fluids, frequently used in industries differs remarkedly from Newtonian fluids. Such fluids are known as non-Newtonian fluids and have extensive utilizations in various fields of engineering and science, such as plastics manufacturing, food processing, wire coating, dying of papers, and glass fibers production, *etc*. The Jeffrey model is one of the most important models of non-Newtonian fluids. The Jeffery fluid model was initially introduced by scientist Jeffery[1] to study the characteristics of viscous fluids. Recently the Jeffrey model has attracted much research because of its applications in many natural areas and industry. Hayat *et al*.[2] reported the three-dimensional (3D) flow behavior of Jeffrey fluid due to nonlinear stretched sheet. Heat and mass transportation in flow of Jeffrey liquid in existence of heat source due to stretched surface is reported by Qasim.[3] Reddy *et al*.[4] investigated flow features of Jeffrey liquid among to torsionally fluctuating disks. Magnetic field on the Jeffrey fluid flow in tubes, having small diameter is reported by Nallapu and Radhakrishnamacharya.[5] For recent developments in Jeffrey fluid interested readers may consult in Refs. [6–11]

A colloidal suspension of nanoparticles (1 nm–100 nm) into base fluids such as water, Ethylene, bio-fluids, oil, and other lubricants, *etc*. is a nanofluid or nanomaterial. Oxide particles, metallic particles, carbon nanotubes, and ceramic particles are commonly used in the formation of nanomaterials. Having higher thermal conductivity and heat transfer rate, nanomaterials have attracted the interest of researchers in the last decade. Hwang *et al*.[12] investigated nanofluids to study their lubrication features and thermal conductivity. Experimental and theoretical investigations were conducted to explore the thermal conductivity and viscosity of nanomaterial flow by Murshed *et al*.[13] Hayat *et al*.[14] inspected the flow features of a Ree–Eyring nanoliquid with a heat source, activation energy, and viscous dissipation between two rotating disks. Khan *et al*.[15] addressed stagnation point flow in cross nanoliquid considering mixed convection, magnetohydrodynamics (MHD), radiation, and activation energy effects. Recent advancements in nanofluids are listed in Refs. [16–23].

The study of fluid flows over a porous-medium surface has gained much attention due to its versatile usages in engineering, industry, bio-engineering, irrigation, blood flow, bio-

†Corresponding author. E-mail: fazal.haq@kiu.edu.pk
© 2022 Chinese Physical Society and IOP Publishing Ltd

physical sciences, and especially in the field of geothermal sciences. Nadeem *et al.*[24] reported Casson fluid flow in three dimensions by a stretching permeable sheet. Xu *et al.*[25] examined the influence of porosity on natural convective transport in fluid flow by metal-foam cavity. Hayat *et al.*[26] examined the impact of porosity on stagnation point flow of magnetohydrodynamic viscous material by a vertical extending sheet. Analysis of heat transportation in the fluid flow due to an exponentially stretched porous surface is reported by Mandal and Mukhopadhyay.[27] The characteristics of the Maxwell fluid over a porous surface is investigated by Bhatti *et al.*[28] Improvement in the thermal performance of nanomaterials in the presence of solid nano-sized particles and foam metals is reported by Xu *et al.*[29,30] Khan *et al.*[31] numerically examined Darcy–Forchhemier flow along with heterogeneous–homogeneous reactions. Mathematical modeling and theoretical investigation of convective nanofluid flow by porous surface with phase interactions is reported by Xing *et al.*[32] Xu *et al.*[33] reported the impacts of permeability on convective heat transportation in fluid flow by metal-foam duct.

The thermal energy per unit temperature that is unavailable for valuable work is the entropy (irreversibility) of system. In other words the total rate of disorder in a system is entropy. In any thermodynamic arrangement, chemical reactions, internal fluid friction, radiation effects, viscous dissipation, magnetic field, porous medium internal energy losses, which generate entropy in the system. Entropy generation gained extraordinary attention in various fields of science and engineering such as heat exchangers, electronic device cooling, and turbomachinery. Poulikakos and Bejan[34] introduced a general framework for irreversibility optimization to study the thermal characteristics of conventional fins of different kinds. In this study the first law of thermodynamics is used to study the different shape of fins and second law of thermodynamics is utilized to optimize the entropy of fins in terms of dimension and length. Latter on Bejan[35] developed a model based on both thermodynamics and system irreversibility. Now, the entropy generation due to nanomaterial flow is becoming an interesting field of research. Wang *et al.*[36] reported Couette flow behavior and estimated entropy generation (EG) for both of heat transfer and shear. Heat transport properties and EG were studied through the second law of thermodynamics and the results obtained are equated with the flow of CuO, Ag, and Al_2O_3 nanoliquid by Jafarmadar *et al.*[37] Khan *et al.*[38] inspected the EG in MHD Carreau nanomaterial flow by a stretched surface subject to viscous dissipation and nonlinear thermal ration. Features of dissipative unsteady flow and EG with thermo-diffusion and diffusion thermo effects are reported by Hayat *et al.*[39] Recent developments on entropy generation are described in Refs. [40–50].

The current work aims to analyze the flow of Jeffrey nanofluid over a stretched configuration with the entropy generation and various thermal features. The motivating and distinct aspects of current analysis are summarized as follows:

(i) Examination of the rheological significances of Jeffrey nanofluid subject to the magnetic force and porous space.

(ii) The applications Bejan number and entropy generation are taken into account with optimized applications.

(iii) The novel significances of viscous dissipation and thermal radiation are also utilized to examine the combined heat/mass transport.

(iv) Convective boundary conditions are imposed to improve the transportation process.

(v) Some studies have already been reported in the literature regarding the flow of Jeffrey nano-materials over a stretched surface, however, the flow of Jeffrey nanofluid in presence of such thermal consequences has not been performed in the literature. Therefore, the current investigation aims to fill this research gap. The solution procedure is based on analytical expressions employing a homotopic convergent scheme.

(vi) Current thermal flow model conveys many applications in the improving heat transfer mechanism, solar energy applications, thermal systems, energy production, energy consumptions, *etc.*

2. Problem formulation

Here MHD two-dimensional convective transport of Jeffrey nano-material with entropy generation assessment is presented with convective boundary constraints. For electrically conducting fluid, the magnetic force impact is assumed in the normal direction with uniform magnetic field strength B_0 as shown in Fig. 1.

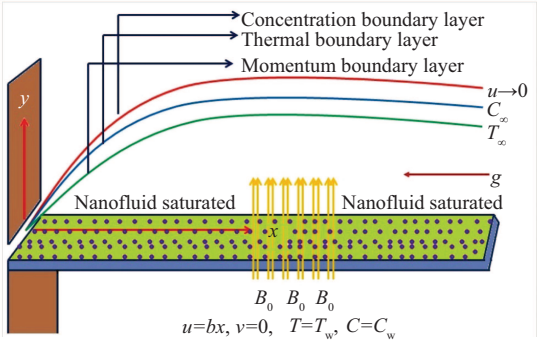


Fig. 1. Flow geometry.

The role of the induced magnetic force is ignored due to small Reynolds number assumptions. Furthermore, the energy equation is modified by considering the viscous dissipa-

tion and thermal radiation. The important prospective of thermophoretic features and Brownian movement are utilized. The linear configuration (stretched surface) attain uniform velocity $u_{\rm w}(x)=bx$. The mathematical model for the Jeffrey nanofluid after employing boundary layer assumptions is given as follows:

$$\frac{\partial u}{\partial x}+\frac{\partial v}{\partial y}=0, \tag{1}$$

$$u\frac{\partial u}{\partial x}+v\frac{\partial u}{\partial y}=\frac{\nu}{1+\lambda_2}\left[\frac{\partial^2 u}{\partial y^2}+\lambda_1\left(u\frac{\partial^3 u}{\partial x\partial y^2}+v\frac{\partial^3 u}{\partial y^3}-\frac{\partial u}{\partial x}\frac{\partial^2 u}{\partial y^2}+\frac{\partial u}{\partial x}\frac{\partial^2 u}{\partial x\partial y}\right)\right]-\frac{\sigma B_0^2}{\rho}u-\frac{\nu}{k_{\rm p}}u, \tag{2}$$

$$\begin{aligned}u\frac{\partial T}{\partial x}+v\frac{\partial T}{\partial y}=&\frac{k}{\rho c_{\rm p}}\frac{\partial^2 T}{\partial y^2}+\tau\left\{D_{\rm B}\frac{\partial C}{\partial y}\frac{\partial T}{\partial y}+\frac{D_{\rm T}}{T_\infty}\left(\frac{\partial T}{\partial y}\right)^2\right\}+\frac{\sigma B_0^2}{\rho c_{\rm p}}u^2-\frac{16\sigma}{3k^*\rho c_{\rm p}}\frac{\partial}{\partial y}\left(T^3\frac{\partial T}{\partial y}\right)\\&+\frac{\nu}{\rho c_{\rm p}(1+\lambda_2)}\left[\left(\frac{\partial u}{\partial y}\right)^2+\lambda_1\left(u\frac{\partial u}{\partial y}\frac{\partial^2 u}{\partial x\partial y}+v\frac{\partial u}{\partial y}\frac{\partial^2 u}{\partial y^2}\right)\right],\end{aligned} \tag{3}$$

$$u\frac{\partial C}{\partial x}+v\frac{\partial C}{\partial y}=D_{\rm B}\frac{\partial^2 C}{\partial y^2}+\frac{D_{\rm T}}{T_\infty}\frac{\partial^2 T}{\partial y^2} \tag{4}$$

with

$$\begin{aligned}&u=u_{\rm w}(x)=ax,\quad -k\frac{\partial T}{\partial y}=h_f(T_{\rm w}-T),\quad v=0,\\&D_{\rm B}\frac{\partial C}{\partial y}+\frac{D_{\rm T}}{T_\infty}\frac{\partial T}{\partial y}=0\ \text{at}\ y=0,\\&u\to u_0(x)=bx,\ T\to T_\infty,\ C\to C_\infty\ \text{as}\ y\to\infty,\end{aligned} \tag{5}$$

where B_0 is the magnetic field, (u,v) is the velocity along x and y directions, $(T_{\rm w},C_{\rm w})$ is the surface temperature and concentration, λ_1 is relaxation time, $D_{\rm B}$ is the coefficient of the Brownian motion, λ_2 is the relaxation to retardation time ratio, $c_{\rm p}$ is fluid specific heat, $k_{\rm p}$ is permeability, $D_{\rm T}$ is the thermophoretic diffusion, ν is the kinematic viscosity, b is the sheet stretching rate constant, (T_∞,C_∞) is the ambient temperature and concentration, k^* is the absorption coefficient, σ is the electric conductivity, τ is the heat capacity ratio, h_f is the convective heat transfer, k is thermal conductivity, $q_{\rm m}$ is the local mass flux, Ha is Hartman number, β is Deborah number, A is the ratio parameter, k_1 is the porosity parameter, $N_{\rm b}$ is Brownian dispersion variable, $R_{\rm d}$ is the radiation parameter, Pr is Prandtl number, $N_{\rm t}$ is thermophoresis variable, Ec is Eckert number, $N_{\rm r}$ is temperature difference ratio parameter, Sc is Schmidt number, Sh_x is Sherwood number, Cf_x is he skin friction, Nu_x is Nusselt number, Re is Reynolds number, Br is Brinkman number, ε is concentration difference variable, Ω is the temperature difference parameter, λ_3 is diffusive variable, Bi is thermal biot number, μ is the dynamic viscosity, η is a dimensionless variable, T is the nanofluid temperature, $\theta(\eta)$ is the dimensionless temperature, $\varphi(\eta)$ is the dimensionless concentration, $f'(\eta)$ is dimensionless velocity, C is the nanofluid concentration, and $q_{\rm w}$ is the surface heat flux. Considering

$$\begin{aligned}&\eta=\sqrt{\frac{a}{\upsilon}}y,\quad u=axf',\quad v=-\sqrt{a\upsilon}f,\\&\theta(\eta)=\frac{T-T_\infty}{T_{\rm w}-T_\infty},\quad \phi(\eta)=\frac{C-C_\infty}{C_{\rm w}-C_\infty}.\end{aligned} \tag{6}$$

Using Eq. (6), equations (2)–(5) take the form

$$f'''-k_1f'(1+\lambda_2)+\left\{ff''-f'^2-Haf'+\beta\left(f''^2-ff^{(iv)}\right)\right\}=0, \tag{7}$$

$$\begin{aligned}&(1+\lambda_2)\theta''+Pr(1+\lambda_2)\left[f\theta'+N_{\rm b}\theta'\phi'+N_{\rm t}\theta'^2+EcHa^2f'^2\right]+R_{\rm d}(1+\lambda_2)\left[3(Nr+1)^2\theta'^2+(Nr+1)^3\theta''\right]\\&\quad+PrEc\left[f''^2+\beta\left(f'f''^2-ff''f'''\right)\right]=0,\end{aligned} \tag{8}$$

$$\phi''+\frac{N_{\rm t}}{N_{\rm b}}\theta''+Scf\phi'=0, \tag{9}$$

$$\begin{aligned}&f(0)=0,\ N_{\rm b}\phi'(0)+N_{\rm t}\theta'(0)=0,\ f'(0)=1,\ \theta'(0)=-B_i(1-\theta(0)),\theta(0)=1\ \text{at}\ \eta=0,\\&f'(\infty)\to A,\ \theta(\infty)\to0,\ \phi(\infty)\to0\ \text{as}\ \eta\to\infty.\end{aligned} \tag{10}$$

Here,

$$\begin{aligned}&Ha=\frac{\sigma B_0^2}{a\rho},\quad \beta=a\lambda_1,\quad A=\frac{b}{a},\quad k_1=\frac{\nu}{ak_{\rm p}},\quad N_{\rm b}=\frac{\tau D_{\rm B}(C_{\rm w}-C_\infty)}{\nu},\quad Sc=\frac{\nu}{D_{\rm B}},\quad Bi=\frac{h_f}{k}\sqrt{\frac{\upsilon}{\rm a}},\\&R_{\rm d}=\frac{16\sigma^*(T_{\rm w}-T_\infty)^3}{3k^*k_{\rm p}},\quad Pr=\frac{\mu c_{\rm p}}{k^*},\quad N_{\rm t}=\frac{\tau D_{\rm T}(T_{\rm w}-T_\infty)}{\nu T_\infty},\quad Ec=\frac{u_{\rm w}^2}{C_{\rm p}(T_{\rm w}-T_\infty)},\quad Nr=\frac{T_\infty}{T_{\rm w}-T_\infty}.\end{aligned} \tag{11}$$

2.1. Physical quantities

The coefficient of skin friction (Cf_x), Sherwood (Sh_x), and Nusselt (Nu_x) numbers are mathematically defined as

$$\begin{aligned} Cf_x &= \frac{2\tau_{\rm w}}{\rho u_{\rm w}^2}, \\ Nu_x &= \frac{x q_{\rm w}}{k_f\left(T_{\rm w}-T_\infty\right)}, \\ Sh_x &= \frac{x j_{\rm w}}{D_{\rm B}\left(C_{\rm w}-C_\infty\right)}, \end{aligned} \tag{12}$$

where

$$\begin{aligned} \tau_{\rm w} &= \frac{\nu}{(1+\lambda_2)}\left[\frac{\partial u}{\partial y}+\lambda_1\left(u\frac{\partial^2 u}{\partial x\partial y}+v\frac{\partial^2 u}{\partial y^2}\right)\right]\Bigg|_{y=0}, \\ q_{\rm w} &= -k\left(1+\frac{16\sigma^*}{3kk^*}T^3\right)\frac{\partial T}{\partial y}\Bigg|_{y=0}, \\ j_w &= -D_{\rm B}\frac{\partial C}{\partial y}\Bigg|_{y=0}. \end{aligned} \tag{13}$$

Using Eq. (12), the dimensionless form of Eq. (11) is

$$\begin{aligned} &Cf_x\left(Re_x\right)^{0.5} = \frac{2}{(1+\lambda_2)}\left\{f''(0)+\beta\left[f'(0)\,f''(0)-f(0)\,f'''(0)\right]\right\}, \\ &Sh_x Re_x^{-0.5} = -\phi'(0), \quad Nu_x Re_x^{-0.5} = -\left\{1+R_{\rm d}\left(\theta(0)+Nr\right)^3\right\}\theta'(0), \end{aligned} \tag{14}$$

where $Re_x\left(=ax^2/\nu\right)$ is the Reynolds number.

2.2. Entropy rate and Bejan number

The local volumetric rate of irreversibility for the considered flow is[9,14,38]

$$\begin{aligned} E_{\rm G} = {} & \frac{k}{T_\infty^2}\left(1+\frac{16\sigma^*}{3kk^*}T^3\right)\left(\frac{\partial T}{\partial y}\right)^2+\frac{\sigma B_0^2}{T_\infty}u^2+\frac{\mu}{T_\infty k_{\rm p}}u^2+\frac{\nu}{\rho c_{\rm p}\left(1+\lambda_2\right)}\left[\left(\frac{\partial u}{\partial y}\right)^2+\lambda_1\left(u\frac{\partial u}{\partial y}\frac{\partial^2 u}{\partial x\partial y}+v\frac{\partial u}{\partial y}\frac{\partial^2 u}{\partial y^2}\right)\right] \\ & +\frac{R_{\rm d}D_{\rm B}}{T_\infty}\frac{\partial T}{\partial y}\frac{\partial C}{\partial y}+\frac{R_{\rm d}D_{\rm B}}{C_\infty}\left(\frac{\partial C}{\partial y}\right)^2. \end{aligned} \tag{15}$$

The first term of Eq. (15) is the entropy generation due to thermal radiation, the second is due to magnetic field, the third is due to the porous medium, the fourth is due to the viscous dissipation, the fifth and sixth terms are due to mass transfer.

The characteristic entropy generation rate $\left(E_{\rm G_0}\right)$ is

$$E_{\rm G_0} = \frac{k\left(T_{\rm w}-T_\infty\right)^2}{T_\infty^2 x^2}. \tag{16}$$

The final form of entropy is

$$\begin{aligned} N_{\rm G} = \frac{E_{\rm G}}{E_{\rm G_0}} = {} & Re\left[1+R_{\rm d}\left\{1+(Nr-1)\,\theta\right\}^3\right]\theta'+\frac{HaReBr}{\lambda_3}f'^2+\frac{k_1 ReBr}{\lambda_3}f'^2 \\ & +\frac{ReBr}{\lambda_3\left(1+\lambda_2\right)}\left[f''^2+\beta\left(f'f''^2-ff''f'''\right)\right]+\frac{Re\varepsilon}{\lambda_3}\theta'\phi'+\frac{Re\varepsilon\Omega^2}{\lambda_3^2}\phi'^2. \end{aligned} \tag{17}$$

Mathematically

$$\begin{aligned} &Re = \frac{u_w x}{\nu},\ Br = \frac{\mu u_{\rm w}^2}{k\left(T_{\rm w}-T_\infty\right)},\ \lambda_3 = \frac{T_{\rm w}-T_\infty}{T_\infty}, \\ &\Omega = \frac{C_{\rm w}-C_\infty}{C_\infty},\ \varepsilon = \frac{R_{\rm d}D_{\rm B}C_\infty}{k}. \end{aligned} \tag{18}$$

The Bejan number is defined as

$$Be = \frac{\text{Entropy generation due to heat transfer}}{\text{Total entropy generation}}, \tag{19}$$

$$Be = \frac{Re\left[1+R_{\rm d}\left\{1+(Nr-1)\,\theta\right\}^3\right]\theta'}{N_{\rm G}}. \tag{20}$$

3. Solution procedure

The set of dimensionless equations (7)–(9) are locally similar so the analytical solution is computed by using the homotopy analysis method (HAM). The pioneer directions and mathematical formulation of this scheme was originally proposed by Liao[51] and later many interesting developments and generalizations on this method have been presented by various researchers.[41,45,48] The relevant initial guesses and linear operators are taken as

$$\begin{aligned} f_0(\eta) &= 1-(1-A)\,{\rm e}^{-\eta}-A(1-\eta), \\ \theta_0(\eta) &= \frac{\beta_i}{1+\beta_i}{\rm e}^{-\eta}, \end{aligned}$$

$$\phi_0(\eta) = \frac{\beta_i}{1+\beta_i}\left(\frac{N_t}{N_b}\right)e^{-\eta}, \tag{21}$$

$$\pounds_f = \frac{d^3 f}{d\eta^3} - \frac{df}{d\eta}, \quad \pounds_\theta = \frac{d^2\theta}{d\eta^2} - \theta,$$

$$\pounds_\phi = \frac{d^2\phi}{d\eta^2} - \phi, \tag{22}$$

with

$$\pounds_f\left[B_1 + B_2 e^{\eta} + B_3 e^{-\eta}\right], \quad \pounds_\theta\left[B_4 e^{\eta} + B_5 e^{-\eta}\right],$$
$$\pounds_\phi\left[B_6 e^{\eta} + B_7 e^{-\eta}\right], \tag{23}$$

where B_i ($i = 1$–7) are constants.

4. Convergence analysis

The assisting variables $\hbar_f$, $\hbar_\theta$, and $\hbar_\phi$ play a vital role in regulating the convergence of homotopic expressions. Figure 2 is plotted to find the ranges of assisting parameters after the 14-th order of approximation when $\lambda_2 = A = \beta = k_1 = 0.1$, $Ec = 0.3$, $Ha = N_t = B_i = 0.2$, $R_d = 0.4$, $N_b = 0.7$, $Sc = Pr = 1.0$, and $Nr = 1.1$.

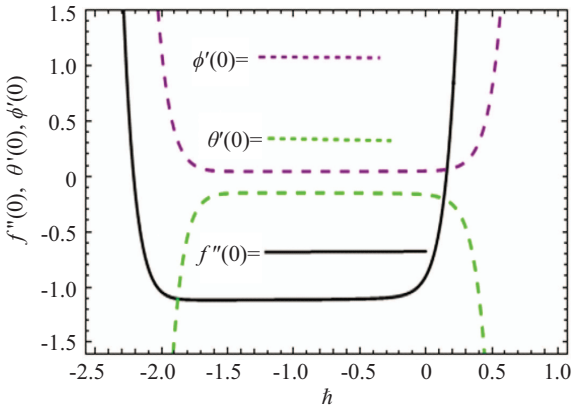


Fig. 2. The $\hbar$ curves for $f''(0)$, $\theta'(0)$, and $\phi'(0)$.

The convergence regions of velocity, temperature, and concentration functions are $-1.8 \le \hbar_f \le -0.4$, $-1.5 \le \hbar_\theta \le -0.3$, and $-1.6 \le \hbar_\phi \le -0.2$. The convergence of the HAM solution is presented in Table 1.

Table 1. Computational outcomes for $f''(0)$, $\phi'(0)$, and $\theta'(0)$, when $\lambda_2 = A = \beta = k_1 = 0.1$, $Ec = 0.3$, $N_b = 0.7$, $R_d = 0.4$, $Sc = Pr = 1.0$, $Ha = N_t = B_i = 0.2$, and $Nr = 1.1$.

Approximations	$-f''(0)$	$-\theta'(0)$	$\phi'(0)$
01	1.076	0.157	0.0449
05	1.106	0.152	0.0436
10	1.112	0.151	0.0431
15	1.115	0.150	0.0430
20	1.117	0.150	0.0429
25	1.118	0.149	0.0428
30	1.119	0.149	0.0427
35	1.119	0.149	0.0427
40	1.119	0.149	0.0427

5. Solution validation

After successfully simulating the analytical expressions in the previous section, we aim here to confirm the computed solution. To this end, the present results have been verified by comparison with the continuation of Turkyilmazoglu[52] in Table 2. There is an excellent agreement between both studies.

Table 2. Comparison of $f''(0)$ with $\lambda_2 = \beta = k_1 = A = 0$.

Ha	Turkyilmazoglu[52]	Present results
0.0	−1.000000	−1.000000
0.5	−1.224744	−1.224747
1.0	−1.414213	−1.414218

6. Discussion

In this section, we scrutinize graphically the effect of sundry variables on the velocity field $f'(\eta)$, temperature $\theta(\eta)$, mass concentration $\phi(\eta)$, Nusselt number $\left(Nu_x Re_x^{-0.5}\right)$, skin friction coefficient $\left(Cf_x Re_x^{0.5}\right)$, and Sherwood number $\left(Sh_x Re_x^{-0.5}\right)$, total irrevesibility rate (N_G), and Bejan number (Be) against various parameters. Since the current analysis is based on theoretical approach, fixed values are assigned to parameters: $\lambda_2 = A = \beta = k_1 = 0.1$, $Ec = 0.3$, $N_b = 0.7$, $Sc = Pr = 1.0$, $Ha = N_t = B_i = 0.2$, $R_d = 0.4$, and $Nr = 1.1$.

6.1. Velocity profile

In this subsection salient features of the Deborah number (β), Hartman number (Ha), permeability parameter (k_1), and ratio parameter (A) on the Jeffery nanofluid velocity $(f'(\eta))$ are discussed. The effect of β on $f'(\eta)$ is shown in Fig. 3(a). The fluid velocity increases *versus* higher β. Physically, β has direct relation with the sheet stretching rate, so increasing β causes an increase in the sheet stretching rate, as a result the fluid velocity inside the boundary layer upsurges and the thickness of momentum boundary layer also increases. Velocity field decays via higher fluid parameter, since fluid parameter has inverse relation with retardation time which means that retardation time decay with higher λ_2 (Fig. 3(b)). A decrease in velocity with increasing Hartman number is observed in Fig. 3(c). Physically, for higher Ha, more Lorentz force is produced, which is a restive force acting on the fluid opposite to the flow. Hence the fluid velocity retards with rising Ha. Figure 3(d) explores the influence of the porosity variable on velocity field. In fact the velocity has an inverse relation with permeability, thus $f'(\eta)$ and momentum layer thickness decease with increasing k_1. The influence of the ratio variable on the velocity is depicted in Fig. 3(e).

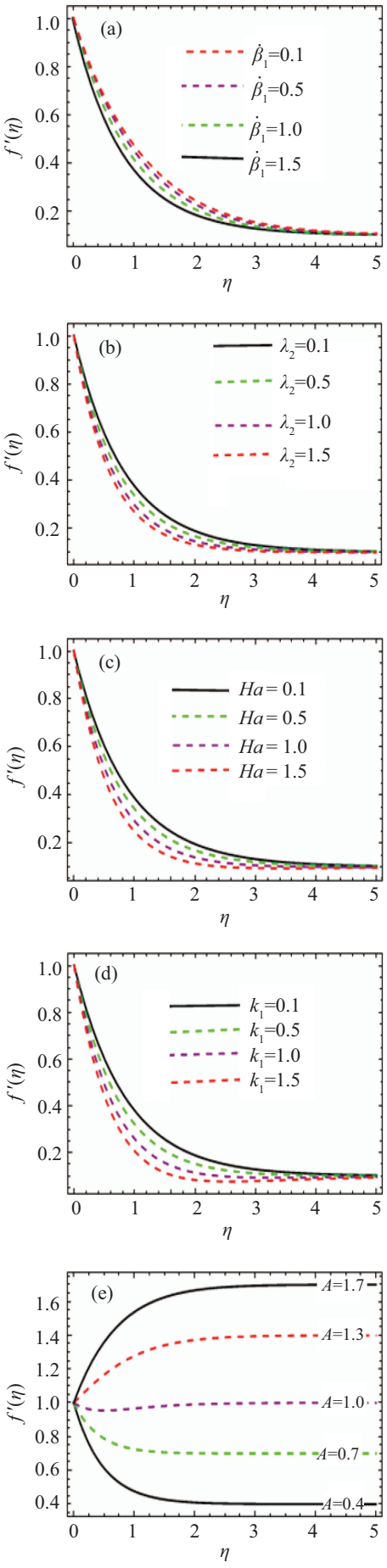


Fig. 3. Impacts β (a), λ_2 (b), Ha (c), k_1 (d), and A (e) on $f'(\eta)$.

It can be seen from this figure that for $A < 1$, the velocity field and the layer thickness increase and for $A > 1$, the velocity decreases and layer thickness increase whereas for $A = 1$ the boundary vanishes since for $A = 1$ the fluid velocity and sheet stretching velocity becomes the same.

6.2. Temperature profile

Figures 4(a)–4(h) presented to show the behavior of the temperature field $\theta(\eta)$ with fluid parameter (λ_2), the Prandtl number (Pr), the thermophoretic variable (N_t), the ratio of temperature (Nr), the Brownian movement (N_b), the radiation parameter (R_d), and the thermal biot number (Bi).

Figure 4(a) explores the characteristics of $\theta(\eta)$ with increasing thermal layer λ_2, the thickness inflates with higher λ_2 since for higher λ_2 retardation time deceases which causes an increase in the temperature field and thermal layer. The variation in $\theta(\eta)$ for higher Pr is depicted in Fig. 4(b). The nanofluid temperature decreases at higher Pr. As we know that Pr has an inverse relation with thermal diffusivity, so an increase in Pr means a decrease in fluid thermal diffusivity. Subsequently thermal field and associated layer width falling down with rising Pr. The radiation effect on the thermal field is studied in Fig. 4(c). As expected the thermal field and layer thickness increase for higher R_d. Physically, the radiation variable describes relation of heat transfer conduction to transfer of thermal radiation, so an increase in R_d slows down the thermal radiation transmission, which ultimately favors temperature increase. The behavior of $\theta(\eta)$ with Ec is displayed in Fig. 4(d). The observations reveal that $\theta(\eta)$ is a decreasing function of Ec.

Figure 4(e) elucidates the impact of the Brownian movement of nanoparticles on the thermal field. Clearly $\theta(\eta)$ increases with higher N_b, because the Brownian phenomenon involves the random movement of nanoparticles which increases with temperature profile. The graphical trend explored in Fig. 4(f) shows an increasing variation in nanofluid temperature due to specified values of N_t. Physically, the thermophoretic force is a force which extracts the nanoparticles from a hot surface and pushes them to a region of low temperature and consequently an improved heat transfer phenomenon results.

Figure 4(g) shows the influence of N_r on $\theta(\eta)$, obviously the thermal field diminishes for higher N_r. Wall temperature (T_w) is higher than ambient temperature and N_r is inversely proportional to $T_w - T_\infty$, thus for higher N_r the $\theta(\eta)$ decreases. Variation of $\theta(\eta)$ with increasing values of Bi is plotted in Fig. 4(h). The nanofluid temperature and thermal layer decreases with higher Bi.

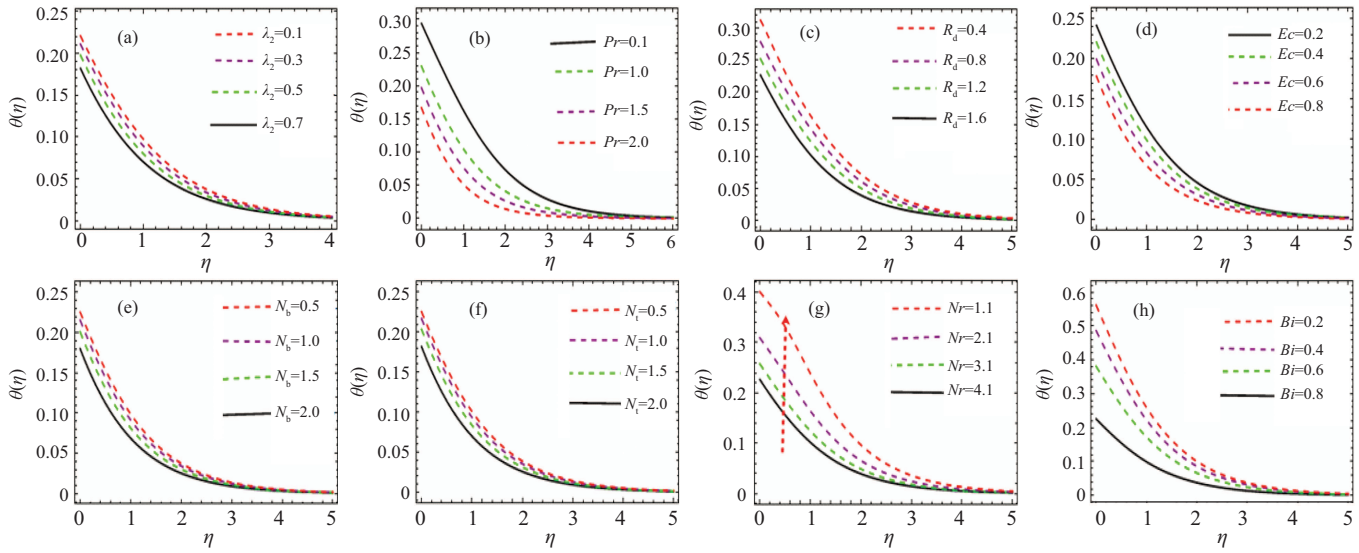


Fig. 4. Impacts of λ_2 (a), Pr (b), R_d (c), Ec (d), N_b (e), N_t (f), Nr (g), and Bi (h) on $\theta(\eta)$.

6.3. Concentration profile

Features of the mass concentration $(\varphi(\eta))$ *versus* Brownian dispersion (N_b), Schmidt number (Sc), and thermophoresis diffusion variable (N_t) are studied in this subsection through Figs. 5(a)–5(c).

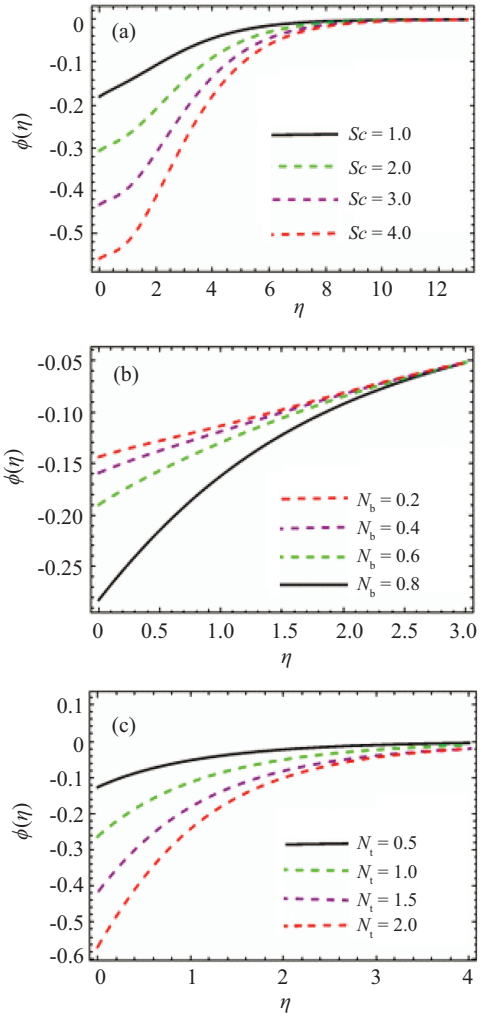


Fig. 5. Impacts of Sc, N_b, and N_t on $\varphi(\eta)$.

The behavior of $\varphi(\eta)$ for increasing Sc in Fig. 5(a) indicates that higher Sc reduces mass concentration. Physically, Sc represents the ratio of momentum to mass diffusivities, so increase in Sc results in an increment in momentum diffusivity while mass diffusivity diminishes. Ultimately a reduction in mass concentrations is observed. Figures 5(b) and 5(c) shows the influence of N_b and N_t on mass concentration. Clearly $\varphi(\eta)$ increases with N_b and diminishes with higher N_t.

6.4. Physical quantities

In this subsection, the behavior of physical quantities, *i.e.*, skin friction (Cf_x), Nusselt number (Nu_x), and local mass transfer (Sh_x) *versus* influential variables are presented graphically.

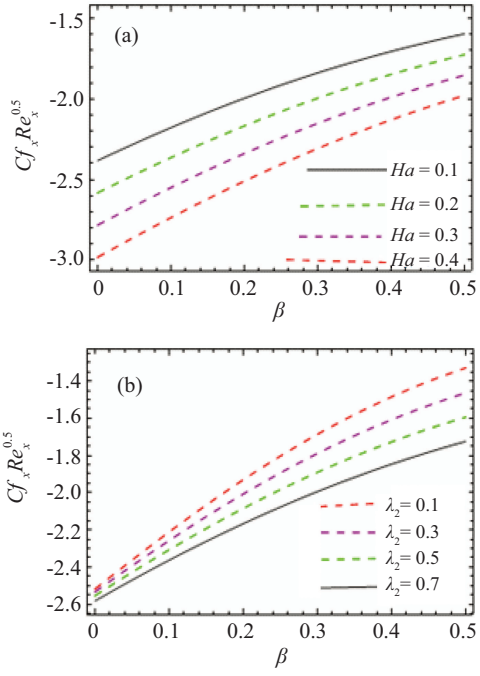


Fig. 6. Effects of Ha and β (a), λ_2 and β (b) on $Cf_x Re_x^{0.5}$.

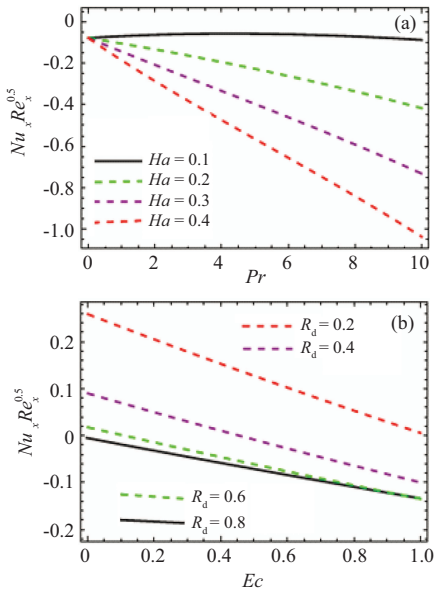


Fig. 7. Effects of Ha and Pr (a), $R_{\rm d}$ and Ec (b) on $Nu_x Re_x^{-0.5}$.

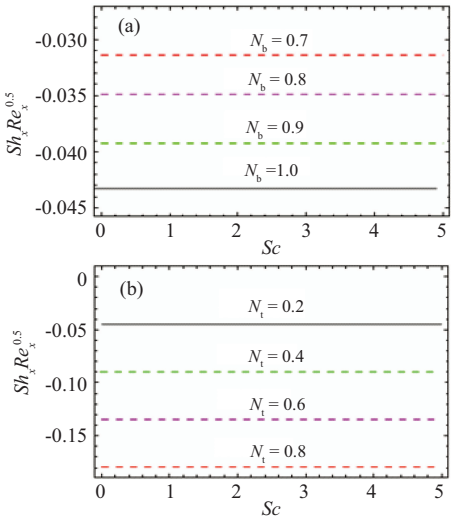


Fig. 8. Effects of $N_{\rm b}$ and Sc (a), $N_{\rm t}$ and Sc on $Sh_x Re_x^{-0.5}$.

The graphical observations presented in Figs. 6(a) and 6(b) reflect the influence of Ha, β, and λ_2 on skin friction. The magnitude of the skin friction diminishes for higher Hartman and Deborah number and Cf_x increases with the fluid parameter and Deborah number. The characteristics of Nu_x *versus* Pr, Ha, $R_{\rm d}$, and Ec are studied through Figs. 7(a) and 7(b). The Nusselt number monotonically decreases for increasing values of Pr and fixed values of Ha (see 7(a)). From Fig. 7(b), it can be seen that the Nusselt number decreases with higher radiation variable and Eckert number. Figures 8(a) and 8(b) explore the behavior of the Sherwood number against $N_{\rm b}$, $N_{\rm t}$, and Sc. The magnitude of the Sherwood number increases with larger $N_{\rm b}$ and Sc while a declining change is noted due to variation of $N_{\rm t}$ and Sc.

6.5. Entropy generation and Bejan number

In this subsection the impact of significant variables on Bejan number (Be) and entropy $(N_{\rm G})$ is analyzed and discussed graphically through Figs. 9(a)–9(f). The influence of Brinkman number on entropy and Bejan number is demonstrated in Figs. 9(a) and 9(b). It is observed from these figures that entropy increases for higher Brinkman number (Br) while the Bejan number decreases. Physically, Brinkman number attains opposite relations with thermal diffusivity which means that maximum values of Br entropy generation increases and the Bejan number decreases. Figures 9(c) and 9(d) demonstrates the behavior of $N_{\rm G}$ and Be for increasing values of Jeffrey fluid variable (λ_2). It is observed from these figures that the trend for both $N_{\rm G}$ and Be is to increase at higher λ_2. Figures 9(e) and 9(f) display the effect of radiation constant $(R_{\rm d})$ on $N_{\rm G}$ and Be. Both $N_{\rm G}$ and Be increase with higher $R_{\rm d}$. In fact $R_{\rm d}$ has direct relation with both $N_{\rm G}$ and Be, so for higher $R_{\rm d}$ radiation emission increases. Consequently $N_{\rm G}$ and Be for higher $R_{\rm d}$.

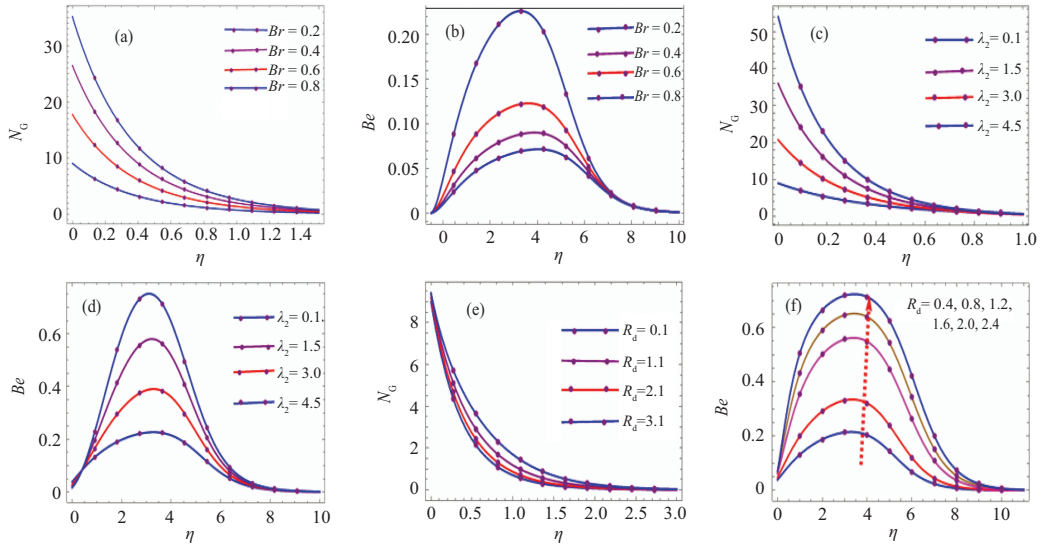


Fig. 9. Behavior of $N_{\rm G}$ and Be *versus* Br, λ_2, and $R_{\rm d}$.

7. Conclusions

The mathematical modeling and analysis for the flow of Jeffrey nanofluid with entropy generation features, Joule heating and thermal radiation has been presented. The porous stretched surface subject to the magnetic force induces the flow. The analytical procedure based on a convergent scheme is followed to compute the solution. The solution accuracy is ensured and compared with previous research data. The summarized observations are listed below.

(i) A declining trend in the velocity profile is observed with permeability of porous space, Deborah number and fluid parameter.

(ii) An increase in nanofluid temperature is related to the Biot number, fluid constant, radiation parameter, and temperature difference ratio parameter.

(iii) The skin friction coefficient decreases with higher Hartmann number and Deborah number while a monotonically increment is noticed for the fluid parameter.

(iv) A lower change in local Nusselt number is observed due to the change in Hartmann number.

(v) A declining impact of Brinkman number on entropy generation and Bejan number is noticed.

(vi) Entropy generation and Bejan number increase with fluid constant and radiation parameter.

Acknowledgment

This research was supported by Taif University Researchers Supporting Project (Grant No. TURSP-2020/217), Taif University, Taif, Saudi Arabia.

References

[1] Jeffery G B 1915 *The London, Edinburgh and Dublin Philosophical Magazine and Journal of Science* **29** 455
[2] Hayat T, Awais M and Obaidat S 2012 *Commun. Nonlinear Sci. Num. Simul.* **17** 699
[3] Qasim 2013 *Alexandria Engineering Journal* **52** 571
[4] Reddy G B, Sreenadh S, Reddy R H and Kavitha A 2015 *Ain Shams Engineering Journal* **6** 355
[5] Nallapu S and Radhakrishnamacharya G 2015 *Procedia Engineering* **127** 185
[6] Waqas M, Shehzad S A, Hayat T, Khan M I and Alsaedi A 2019 *J. Phys. Chem. Solids* **133** 45
[7] Yasmeen S, Asghar S, Anjum H J and Ehsan T 2019 *Commun. Nonlinear Sci. Num. Simul.* **76** 51
[8] Chakraborty T, Das K and Kundu P K 2017 *Journal of Molecular Liquids* **229** 443
[9] Gul A, Khan I and Makhanov S S 2018 *Results in Physics* **9** 947
[10] Hasona W M, El-Shekhipy A A and Ibrahim M G 2018 *Int. J. Heat Mass Transfer* **126** 700
[11] Hayat T, Asad S, Mustafa T and Alsaedi A 2015 *Computers and Fluids* **108** 179
[12] Hwang Y, Park H S, Lee J K and Jung W H 2006 *Current Applied Physics* **6** e67
[13] Murshed S M S, Leong K C and Yang C 2008 *Int. J. Thermal Sci.* **47** 560
[14] Qayyum S, Khan M I, Hayat T, Alsaedi A and Tamoor M 2018 *Int. J. Heat Mass Transfer* **127** 933
[15] Khan M I, Hayat T, Khan M I and Alsaedi A 2008 *Int. Commun. Heat Mass Transfer* **91** 216
[16] Alsaedi A, Khan M I, Farooq M, Gull N and Hayat T 2017 *Adv. Powder Technol.* **28** 288
[17] Kumar A and Subudhi S 2019 *Appl. Thermal Eng.* **160** 114092
[18] Yldz C, Arc M and Karabay H 2019 *Int. J. Heat Mass Transfer* **140** 598
[19] Assael M J, Antoniadis K D, Wakeham W A and Zhang X 2019 *Int. J. Heat Mass Transfer* **138** 597
[20] Sheikholeslami M, Hayat T and Alsaedi A 2017 *Int. J. Heat Mass Transfer* **115** 981
[21] Sheikholeslami M, Hayat T and Alsaedi A 2018 *J. Mol. Liquids* **249** 941
[22] Tong Y, Lee H, Kang W and Cho H 2019 *Appl. Thermal Eng.* **159** 113959
[23] Turkyilmazoglu M 2019 *Eur. J. Mech.-B Fluids* **76** 1
[24] Nadeem S, Haq R U, Akbar N S and Khan Z H 2013 *Alexandria Engineering J.* **52** 577
[25] Xu H and Xing Z 2017 *Int. Commun. Heat Mass Transfer* **89** 73
[26] Hayat T, Abbas Z, Pop I and Asghar S 2010 *Int. J. Heat Mass Transfer* **53** 466
[27] Mandal I C and Mukhopadhyay S 2013 *Ain Shams Engineering J.* **4** 103
[28] Bhatti M M, Shahid A and Rashidi M M 2016 *Alexandria Engineering J.* **55** 51
[29] Xu H, Xing Z and Vafai K 2019 *Int. J. Heat Fluid Flow* **77** 242
[30] Xing Z B, Han X, Ke H, Zhang Q G, Zhang Z and Xu H F 2021 *Int. J. Num. Methods Heat Fluid Flow* **31** 2754
[31] Khan M I, Hayat T and Alsaedi A 2017 *Results in Physics* **7** 2644
[32] Xu H, Gong L, Huang S and Xu M 2015 *Int. J. Heat Mass Transfer* **83** 399
[33] Xu H, Xing Z B, Wang F Q and Cheng Z M 2019 *Chem. Eng. Sci.* **195** 462
[34] Poulikakos D and Bejan A 1982 *J. Heat Transfer* **104** 616
[35] Bejan A 1996 *Revue Générale de Thermique* **35** 637
[36] Wang Y, Chen Z and Ling X 2015 *Int. J. Heat Mass Transfer* **90** 499
[37] Jafarmadar S, Azizinia N, Razmara N and Mobadersani F 2016 *Appl. Thermal Eng.* **103** 356
[38] Khan M I, Kumar A, Hayat T, Waqas M and Singh R 2019 *J. Mol. Liquids* **278** 677
[39] Hayat T, Sajjad L, Khan M I, Khan M I and Alsaedi A 2019 *J. Mol. Liquids* **282** 557
[40] Seyyedi S M, Dogonchi A S, Hashemi-Tilehnoee M, Asghar Z, Waqas M and Ganji D 2019 *J. Mol. Liquids* **287** 110863
[41] Khan W A, Khan M I, Hayat T and Alsaedi A 2018 *Physica B* **534** 113
[42] Bahmanyar M E and Talebi S 2019 *Ann. Nucl. Energy* **125** 212
[43] Hayat T, Khan M I, Qayyum S, Alsaedi A and Khan M I 2018 *Phys. Lett. A* **382** 749
[44] Huang Q, Tang A, Cai T, Zhao D and Zhou C 2019 *Chem. Eng. Proc.-Process Intensification* **143** 107601
[45] Khan M I, Qayyum S, Hayat T, Khan M I, Alsaedi A and Khan T A 2018 *Phys. Lett. A* **382** 2017
[46] Khan M I, Shah F, Hayat T and Alsaedi A 2019 *Physica A* **527** 121154
[47] Lou C and Zhang Z 2019 *J. Quantitative Spectroscopy and Radiative Transfer* **232** 27
[48] Hayat T, Khan S A, Khan M I and Alsaedi A 2019 *Computer Methods and Programs in Biomedicine* **177** 57
[49] Liu M, Li S, Wu Z, Zhang K, Wang S and Liang X 2019 *Eur. J. Mech. B: Fluids* **77** 87
[50] Khan M I, Alsaedi A, Hayat T and Khan N B 2019 *Computer Methods and Programs in Biomedicine* **179** 104973
[51] Liao S and Sherif S A 2004 *Appl. Mech. Rev.* **57** 25
[52] Turkyilmazoglu M 2013 *Int. J. Mech. Sci.* **77** 263